

Localization and Kosterlitz-Thouless Transition in Disordered Graphene

Yan-Yang Zhang,¹ Jiangping Hu,¹ B.A. Bernevig,² X.R. Wang,³ X.C. Xie,^{4,5} and W.M. Liu⁴

¹ *Department of Physics, Purdue University, West Lafayette, Indiana 47907, USA*

² *Princeton Center for Theoretical Science, Jadwin Hall, Princeton University, Princeton, NJ 08544*

³ *Physics Department, The Hong Kong University of Science and Technology, Clear Water Bay, Hong Kong SAR, China.*

⁴ *Institute of Physics, Chinese Academy of Sciences, Beijing 100080, China.*

⁵ *Department of Physics, Oklahoma State University, Stillwater, Oklahoma 74078, USA*

(Dated: February 10, 2022)

We investigate disordered graphene with strong long-range impurities. Contrary to the common belief that delocalization should persist in such a system against any disorder, as the system is expected to be equivalent to a disordered two-dimensional Dirac Fermionic system, we find that states near the Dirac points are localized for sufficiently strong disorder and the transition between the localized and delocalized states is of Kosterlitz-Thouless type. Our results show that the transition originates from bounding and unbounding of local current vortices.

PACS numbers: 71.30.+h, 72.10.-d, 72.15.Rn, 73.20.Fz

It is well-known that the electronic spectrum of graphene can be approximately described by relativistic Dirac Fermions[1, 2]. This is due to the linear dispersion relation at low energies near two valleys associated to two inequivalent points \mathbf{K} and \mathbf{K}' at the corner of the Brillouin zone[3]. The relativistic dispersion gives rise to several remarkable phenomena. Unlike non-relativistic Schrödinger fermions in two dimensions [9], Dirac fermions cannot be trapped by a barrier due to the Klein paradox, a property of relativistic quantum mechanics[4]. Theories based on the two-dimensional (2D) single flavor Dirac Hamiltonian also predict that Dirac fermions cannot be localized by disorder[5, 6, 7, 8].

The great majority of experimental and theoretical studies of graphene [2, 10] has focused on the effect of the relativistic electronic dispersion on different phenomena such as Landau level structure or quantum Hall ferromagnetism. However, the validity of single flavor Dirac fermion picture for disordered graphene is only approximate and relies on two premisses: (1) The spatial range of the impurities is long enough to avoid inter-valley scattering[5] (for short-range impurities, strong inter-valley scattering can lead to localization[5, 11, 12]); (2) Even in a disordered graphene with long-range impurities that completely suppress inter-valley scattering, a single valley Dirac Hamiltonian is only valid when weak impurities are considered. Since the approximated linear relativistic dispersion is valid near the Dirac valley points, \mathbf{K} and \mathbf{K}' , the approximation cannot be carried out in a region with a strong impurity where the deviation from the Dirac point is large enough so that higher order corrections to the energy spectrum become relevant[5]. Therefore, the application of single valley Dirac Hamiltonian to disordered graphene is limited to weak long-range impurities. Indeed, localized states in disordered graphene near Dirac points have been observed experimentally [13] and numerically[14, 15]. All the above beg the physical question: how does graphene behave in the presence of

strong long-range impurities?

In this letter we investigate several novel phenomena induced by disorder with strong long-range impurities in graphene. We calculate the scaling properties of disordered graphene in the framework of a tight-binding model and finite-size scaling. Instead of delocalization we find that, in the presence of strong long-range impurities, states near the Dirac points are localized. Localization arises from enhanced backscattering due to the deviation from linear dispersion in the strong impurity regime. We show that there is a metal-insulator transition (MIT) as a function of the disorder strength and chemical potential. On the delocalized (metallic) side, the conductance is independent of the system size, which is a characteristic of the Kosterlitz-Thouless (K-T) [16] type transition in conventional 2D systems with random magnetic field [18, 19] or correlated disorder [20]. We verify the Kosterlitz-Thouless transition nature of the MIT by explicitly identifying the bounding and unbounding vortex-anti-vortex local currents in the system.

The π electrons in graphene are described by the tight binding Hamiltonian (TBH)

$$H = \sum_i V_i c_i^\dagger c_i + t \sum_{\langle i,j \rangle} (c_i^\dagger c_j + \text{H.c.}), \quad (1)$$

where c_i^\dagger (c_i) creates (annihilates) an electron on site i with coordinate \mathbf{r}_i , t ($\sim 2.7\text{eV}$) is the hopping integral between the nearest neighbor carbon atoms with distance $a/\sqrt{3}$ ($a \sim 2.46\text{\AA}$ is the lattice constant), and V_i is the potential energy. In the presence of disorder, V_i is the sum of contributions from N_I impurities randomly centered at $\{\mathbf{r}_m\}$ among N sites $V_i = \sum_{m=1}^{N_I} U_m \exp(-|\mathbf{r}_i - \mathbf{r}_m|^2/(2\xi))$, where U_m is randomly distributed within $(-W/2, W/2)$ in units of t . Different random configurations of graphene samples with same size, ξ , W and $n_i \equiv N_I/N$ constitute an ensemble with definite disorder strength. This model has been widely used in investigating the transport properties in graphene[21, 22, 23].

At zero temperature, the two terminal dimensionless conductance g_L of the sample between perfect leads at Fermi energy E_F can be written in terms of Landauer-Büttiker formula [24]:

$$g_L(E_F) = 2\text{Tr}(tt^\dagger), \quad (2)$$

where t is the transmission matrix and the factor 2 accounts for spin degeneracy. Equation (2) can be numerically evaluated by recursive Green's function method [25] for systems with rather large size. For the purpose of scaling, the contact effect should be subtracted from g_L to yield the “intrinsic conductance”, g , defined as $1/g = 1/g_L - 1/(2N_C)$, where N_C is the number of propagating channels at Fermi energy E_F and $1/(2N_C)$ is the contact resistance[26]. The conductance g then receives contributions solely from the bulk and thus has the same scaling property as if it were obtained by the transfer matrix method [27]. The scaling function[9, 27]

$$\beta = \frac{d\langle \ln g \rangle}{d \ln L}, \quad (3)$$

$\langle \dots \rangle$ being the average over random ensemble, is used to determine the localization properties; $\beta < 0$ and $\beta > 0$ correspond to the insulator and the metal, respectively.

We plot the size dependence of $\langle \ln g \rangle$ with $\xi = 1.73a$, $n_I = 1\%$, for different E_F and W in Fig. 1. The samples are set to be square shaped with length L . Periodic boundary conditions in the transverse direction are adopted to exclude the edge states of the zigzag edges[22]. The potential range ξ here is chosen long enough to avoid obvious inter-valley scattering [5, 22], and the scaling $\xi/L_x \sim 0$ is irrelevant. When $E_F < E_c = 0.1t$ (Fig. 1 (a)) or $W > W_c = 2t$ (Fig. 1 (b)), $\langle g \rangle$ is monotonically decreasing with increasing L , which means the wavefunctions are localized. Otherwise, when $E_F > E_c = 0.1t$ (Fig. 1 (a)) or $W < W_c = 2t$ (Fig. 1 (b)), $\langle \ln g \rangle$ curves for different sizes merge, suggesting a delocalized state with finite conductance in the thermodynamic limit. However, they are not real metals with $\beta > 0$. All the states with $W \in (0, W_c)$ are within the metal-insulator transition (MIT) region with $\beta = 0$. Even in the cases of extremely weak disorder with $W = 0.25t$ and $W = 0.1t$ (see the inset of Fig. 1 (b)), except for a vanishing even-odd like fluctuation, $\langle \ln g \rangle(L)$ doesn't seem to show a tendency to be increasing nor decreasing. In Fig. 2, the universal $\beta(\ln g)$ is plotted from the same data in Fig. 1, showing a critical conductance $\ln g_c \sim 1$ separating the delocalized states with $\beta = 0$ and localized states with $\beta < 0$. This phenomenon corresponds to a disorder-driven Kosterlitz-Thouless (K-T) type transition that has been observed in many disordered 2D systems[17, 18, 19, 20]. As can be seen from Fig. 1 (a) and the phase diagram (inset of Fig. 2), states in the low energy region are more easily localized.

The existence of localized states near the Dirac point is in contrast to the belief that Dirac fermions are robust

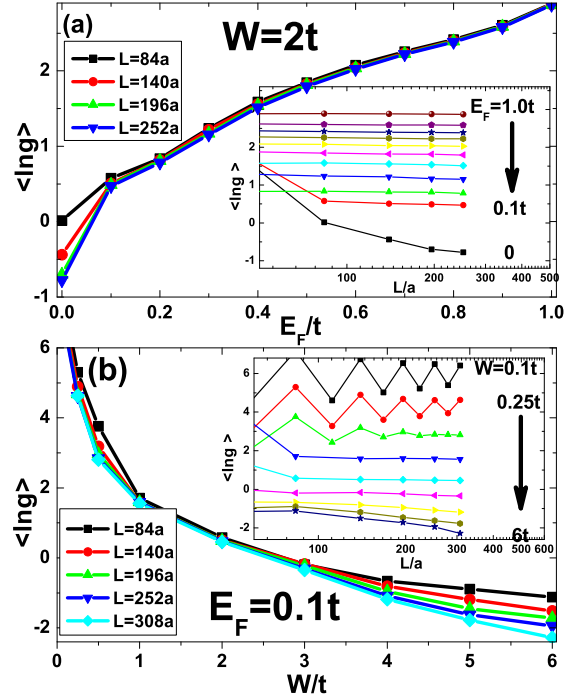


FIG. 1: (Color online) The scaling of conductance for long range disorder ($\xi = 1.73a$, $n_I = 1\%$): (a) $\langle \ln g \rangle$ as functions of the Fermi energy E_F with fixed disorder strength $W = 2t$ (note: the bandwidth is $6t$); (b) $\langle \ln g \rangle$ as functions of disorder strength W with fixed Fermi energy $E_F = 0.1t$. The insets are the same data plotted as functions of size L . Each $\langle \ln g \rangle$ is an average over 100 ~ 400 random realizations.

against localization, especially in the presence of long range impurities that can effectively prohibit the inter-valley scattering. In order to gain insight in the nature of the localization transition, we now turn back to the dispersion structure of realistic graphene. In the absence of disorder ($V_i \equiv 0$), the upper (+) and the lower (−) bands touch at two Dirac points $\mathbf{K} = (\frac{2\pi}{3a}, \frac{2\pi}{3\sqrt{3}a})$ and $\mathbf{K}' = (\frac{2\pi}{3a}, -\frac{2\pi}{3\sqrt{3}a})$. When $|E| \leq t$, the dispersion consists of two valleys centered at Dirac points. Near each Dirac point, e.g. \mathbf{K} , the energy bands can be expanded as[5]

$$E_{\pm}(\mathbf{q}) = \pm \frac{3ta}{2}|\mathbf{q}| \pm \frac{\sqrt{3}ta^2}{8}\sin(3\alpha(\mathbf{q}))|\mathbf{q}|^2 + O(q^3), \quad (4)$$

where $\mathbf{q} \equiv \mathbf{k} - \mathbf{K}$ is the momentum measured from \mathbf{K} and $\alpha(\mathbf{q}) \in [0, 2\pi)$ is the angle of vector \mathbf{q} . The first term in the r.h.s of (4) corresponds to the Dirac Hamiltonian, but non-linear terms will be prominent when \mathbf{q} (or E) is increased. Even when $|E| < t$, the second term in (4) can lead to non-trivial consequences. First, the quadratic dependence on momentum $|\mathbf{q}|^2$ gives rise to non-vanishing backscattering probability and thus a tendency to localization. Second, the angular dependence factor $\sin(3\alpha(\mathbf{q}))$ (“trigonal warping”) breaks the perfect symmetry of the cone-like valley. The pseudo-time rever-

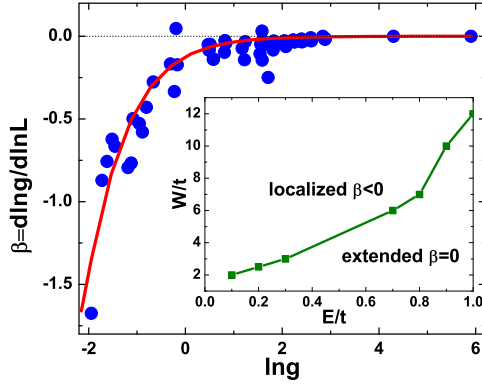


FIG. 2: (Color online) The scaling function $\beta = \frac{d(\ln g)}{d \ln L}$ obtained from the data in Fig. 1. The inset is the schematic phase diagram for $\xi = 1.73a$, $n_I = 1\%$.

sal symmetry [8, 22] restricted to each valley is destroyed. When $|E| > t$, the linear approximation and double-valley structure collapses completely. Although graphene cannot be experimentally doped to a bulk Fermi energy far away from the neutral point (Dirac points) (e.g., $E_F \sim t$), the local potential of impurities might still be high enough to create non-Dirac scatterings. The observed localization originates from the non-Dirac behavior due to higher order corrections to the dispersion.

To confirm this, let us consider the simplest case of a single long range impurity in the center of a graphene sheet. If inter-valley interaction is effectively prohibited and the regime of Klein tunneling[4] holds, there should be no bound states, no matter how high the potential barrier is. After diagonalizing the Hamiltonian for a graphene sheet with N sites, the spatial extension of eigenstate $|\psi_n\rangle = \sum_{i=1}^N a_{ni} c_i^\dagger |0\rangle$ with eigen-energy E_n can be characterized by the participation ratio

$$R_n = \left(\sum_{i=1}^N a_{ni}^2 \right)^2 / \left(N \sum_{i=1}^N a_{ni}^4 \right), \quad (5)$$

which is a measure of the portion of the space where the amplitude of wavefunction differs markedly from zero. For an extended state, R has a finite value (typically close to $1/3$ in the presence of disorder), whereas for a localized state R approaches zero proportional to $(1/N)$ [28]. The results for $\xi = 1.73a$ with different potential height $V \geq 0$ is plotted in Fig. 3. For small V (Fig. 3 (a) and (b)), where the electronic behaviors inside and outside the barrier are Dirac-like (Fig. 3 (e) and (f)), there are no bound states. When V is increased, bound states with small R begin to appear in the negative energy region near the Dirac point, as seen in Fig. 3 (c). For positive injected energy (orange arrow with solid line in Fig. 3 (g)), the electron is not far from \mathbf{K} both inside and outside the barrier, so the regime of Klein tunneling is still valid and the electron cannot be trapped.

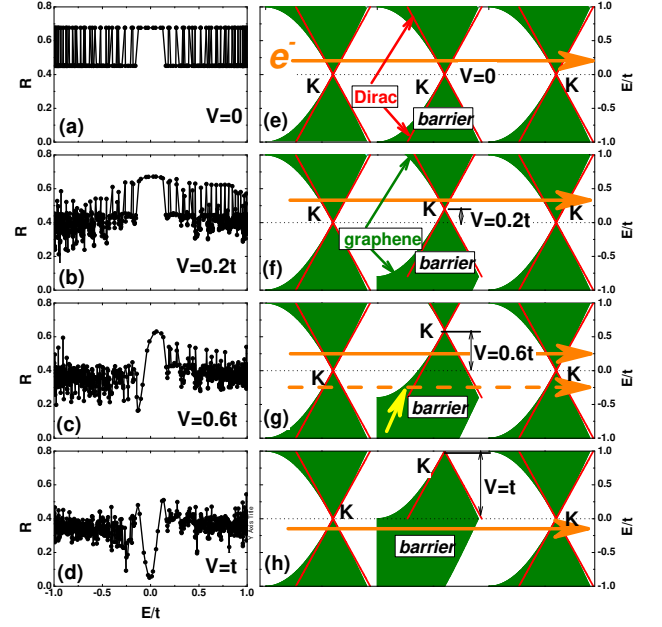


FIG. 3: (Color online) Left column ((a)→(d)): The participation ratio R as functions of energy E for a graphene with $N = 70 \times 40$, in the presence of a single impurity at the center with $\xi = 1.73a$ (long range) with different potential height $V \geq 0$. Right column ((e)→(h)): Schematic diagrams of scattering process corresponding to their left counterparts. The electron is injected from the left, scattered by the barrier at the center and eventually transmitted to the right (thick orange arrows). The dispersion configurations in these three regions around \mathbf{K} are plotted, where the red lines mark the ideal Dirac dispersion $E_{\pm}(\mathbf{k}) = \pm \frac{3ta}{2} |\mathbf{k} - \mathbf{K}|$ and the olive part is that for graphene calculated from TBH. Discrepancies between them at high energy can be clearly seen.

On the other hand, for negative energy (orange arrow with dashed line in Fig. 3 (g)), the electron sees a non-Dirac barrier (pointed by the yellow arrow). This causes strong back-scattering and localization around the impurity. When V is increased further (Fig. 3 (h)), even electrons in the positive Dirac region will encounter strong back-scattering in the barrier and will be localized (Fig. 3 (d)). For negative V (not shown here), all the results are similar, except that the localized states now first appear in the positive region near Dirac point. In conclusion, the localized states originate from back-scattering at the barrier due to its deviation from Dirac behavior at the Fermi level. The states near the Dirac point with low density of states will be more sensitive to backscattering and will be localized first, as in the case of conventional disordered systems[25, 26, 27].

Why is the MIT in disordered graphene of K-T type? The K-T transition is a typical topological transition which has been understood as unbounding of vortex-anti-vortex pairs [16]. For instance, in the high temperature phase 2D XY model, a plasma of unbounded vortices and anti-vortices of local spins gives rise to an exponential de-

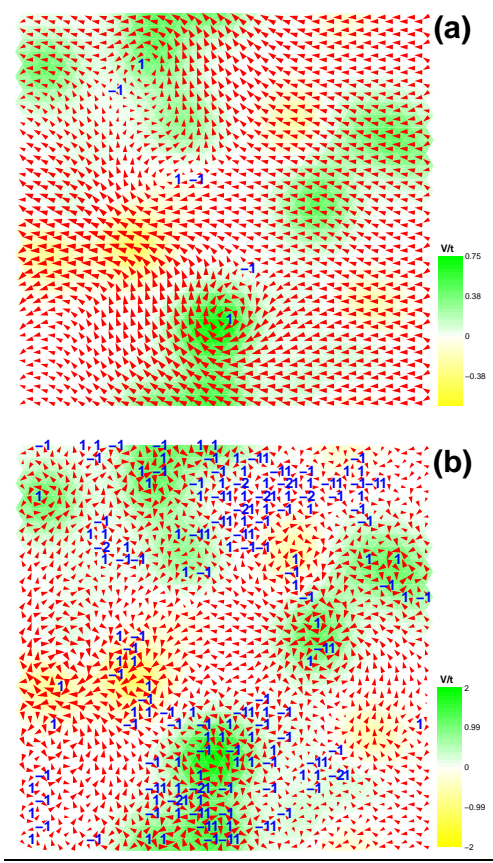


FIG. 4: (Color online) Typical configurations of local currents \mathbf{i}_n (red arrows) and potential V_n (color contour) on two sides of K-T type MIT with $N = 56 \times 32$ sites, $\xi = 1.73a$, $n_I = 1\%$ and $E_F = 0.1t$. (a): $W = 1.1t$ (delocalized); (b): $W = 2.9t$ (localized). The size of arrows is proportional to the logarithm of current value. Carbon hexagons with topological charge $n \neq 0$ are marked explicitly with blue numbers. Both plots are in the same random realization of impurities, with different potential height therefore effectively different W .

cay of spin correlation function; in the low temperature phase, vortices and anti-vortices are bound to each other, leading to a power law correlation function. This can be clearly seen in the present problem if the local currents are identified with local spins in XY model.

The bond current vector $\mathbf{i}_{l \rightarrow m}(E_F)$ per unit energy pointing along the bond between sites l and m can be calculated using Green's functions[24, 29, 30]. It is more convenient to investigate the “current flow vector” $\mathbf{i}_l = \sum_m \mathbf{i}_{l \rightarrow m}$ defined on site l , where the vectorial summation is taken over the nearest neighbors of site l [29]. The current flow \mathbf{i}_l is a vector with angle $\theta_l \in [0, 2\pi)$. The topological charge n of local currents on a closed path can now be defined as usual: $n = \frac{1}{2\pi} \oint \nabla \theta \cdot d\mathbf{l}$. In Fig. 4, typical distributions of local currents on both sides of MIT are plotted. As expected from the K-T picture, in the delocalized phase (Fig. 4 (a)), vortices ($n > 0$) and

anti-vortices ($n < 0$) are closely bounded, corresponding to the “low temperature” phase of 2D XY model with quasi-long range correlations. In the localized phase (Fig. 4 (b)), there are a large number of current vortices and anti-vortices. Many of them are unbounded, corresponding to the “high temperature” phase of 2D XY model without long range correlations. This offers an explicit picture of the microscopic origin of the disorder driven K-T transition in graphene.

In conclusion, we find a Kosterlitz-Thouless type metal-to-insulator transition as a function of disorder strength or Fermi energy in disordered graphene with strong long-range impurities. We explicitly demonstrate the KT nature of transition by showing the bounding and unbounding of local current vortexes. One unique feature about the K-T transition is a scaling of exponential form near the transition point. The conductance $g \propto \exp(-\frac{\alpha}{\sqrt{W-W_c}})$ where α is a constant. Recently, the MIT near the neutral point of graphene has been observed in graphene nanoribbons[13] which are quasi-one-dimensional systems. Our results can be tested in experiments with large nanoribbon radius.

We thank D.-X. Yao, W.-F. Tsai and C. Fang for useful discussions. YYZ and JPH were supported by the NSF under grant No. PHY-0603759.

-
- [1] P. R. Wallace, Phys. Rev. **71**, 622 (1947).
 - [2] K. S. Novoselov *et al.*, Science **438**, 197 (2005).
 - [3] C. K. Kane, Nature **438**, 168 (2005).
 - [4] M. I. Katsnelson *et al.*, Nature Phys. **2**, 620 (2006).
 - [5] T. Ando and T. Nakanishi, J. Phys. Soc. Jpn. **67**, 1704 (1998); T. Ando *et al.*, *ibid.* **67**, 2857 (1998).
 - [6] K. Ziegler, Phys. Rev. Lett. **80**, 3113 (1998).
 - [7] J. H. Bardarson *et al.*, Phys. Rev. Lett. **99**, 106801 (2007).
 - [8] K. Nomura *et al.*, Phys. Rev. Lett. **99**, 146806 (2007).
 - [9] E. Abrahams *et al.*, Phys. Rev. Lett. **42**, 673 (1979).
 - [10] B. Huard *et al.*, Phys. Rev. Lett. **98**, 236803 (2007).
 - [11] A. Atland, Phys. Rev. Lett. **97**, 236802 (2006).
 - [12] S.-J. Xiong and Y. Xiong, Phys. Rev. B **76**, 214204 (2007).
 - [13] S. Adam *et al.*, Phys. Rev. Lett. **101**, 046404 (2008).
 - [14] V. M. Pereira *et al.*, Phys. Rev. Lett. **96**, 036801 (2006).
 - [15] M. Amini *et al.*, arXiv:cond-mat/0806.1329 (2008).
 - [16] J. M. Kosterlitz and D. J. Thouless, J. Phys. C: Solid State Phys. **6**, 1181 (1973).
 - [17] V. Kalmeyer *et al.*, Phys. Rev. B. **48**, 11095 (1993); S.-C. Zhang and D. P. Arovas, Phys. Rev. Lett. **72**, 1886 (1994).
 - [18] X. C. Xie *et al.*, Phys. Rev. Lett. **80**, 3563 (1998).
 - [19] W.-S. Liu *et al.*, Phys. Rev. B **60**, 5295 (1999).
 - [20] W.-S. Liu *et al.*, J. Phys.: Condens. Matter **11**, 6883 (1999).
 - [21] A. Rycerz *et al.*, Europhys. Lett. **79**, 57003 (2007).
 - [22] K. Wakabayashi *et al.*, Phys. Rev. Lett. **99**, 036601 (2007).
 - [23] C. H. Lewenkopf *et al.*, Phys. Rev. B **77**, 081410(R)

- (2008).
- [24] S. Datta, *Electronic Transport in Mesoscopic Systems* (Cambridge University Press, Cambridge, U.K., 1995).
- [25] A. MacKinnon, Z. Phys. B - Condensed Matter **59**, 385 (1985).
- [26] D. Braun *et al.*, Phys. Rev. B **55**, 7557 (1997).
- [27] K. Slevin *et al.*, Phys. Rev. Lett. **86**, 3594 (2001).
- [28] J. T. Edwards and D. J. Thouless, J. Phys. C **5**, 807 (1972).
- [29] L. P. Zârbo and B. K. Nikolić, Europhys. Lett. **80**, 47001 (2007).
- [30] Y. Y. Zhang *et al.*, Phys. Rev. B **78**, 155413 (2008).